Published in final edited form as:
Neuroimage. 2014 December ; 103: 235–240. doi:10.1016/j.neuroimage.2014.09.052.

Integrated RF/shim coil array for parallel reception and localized B_0 shimming in the human brain

Trong-Kha Truong, **Dean Darnell**, and **Allen W. Song**
Brain Imaging and Analysis Center, Duke University, Durham, NC, USA

Abstract

The purpose of this work was to develop a novel integrated radiofrequency and shim (RF/shim) coil array that can perform parallel reception and localized B_0 shimming in the human brain with the same coils, thereby maximizing both the signal-to-noise ratio and shimming efficiency. A 32-channel receive-only head coil array was modified to enable both RF currents (for signal reception) and direct currents (for B_0 shimming) to flow in individual coil elements. Its in vivo performance was assessed in the frontal brain region, which is affected by large susceptibility-induced B_0 in homogeneities. The coil modifications did not reduce their quality factor or signal-to-noise ratio. Axial B_0 maps and echo-planar images acquired in vivo with direct currents optimized to shim specific slices showed substantially reduced B_0 inhomogeneities and image distortions in the frontal brain region. The B_0 root-mean-square error in the anterior half of the brain was reduced by 60.3% as compared to that obtained with second-order spherical harmonic shimming. These results demonstrate that the integrated RF/shim coil array can perform parallel reception and localized B_0 shimming in the human brain and provide a much more effective shimming than conventional spherical harmonic shimming alone, without taking up additional space in the magnet bore and without compromising the signal-to-noise ratio or shimming performance.

Keywords

RF coil; shim coil; coil array; B_0 shimming; human brain

1. Introduction

Magnetic susceptibility differences at air/tissue interfaces induce macroscopic static magnetic field (B_0) inhomogeneities, most prominently in the inferior frontal and temporal brain regions (Truong et al., 2002), resulting in image artifacts such as distortions, blurring, and signal loss, which hamper the investigation of these regions with many applications like

Corresponding Author: Trong-Kha Truong, Ph.D., Brain Imaging and Analysis Center, Duke University Medical Center, 2424 Erwin Road, Suite 501, Durham, NC 27705, USA, Phone: (919) 684-1216, Fax: (919) 681-7033, trongkha.truong@duke.edu.

functional MRI or diffusion tensor imaging. These strong and localized B_0 inhomogeneities cannot be effectively shimmed with conventional whole-body spherical harmonic (SH) shim coils (Romeo and Hoult, 1984), which are typically limited to the second or third order.

Extending from an early work using a few localized shim coils (Hsu and Glover, 2005), multicoil shimming with a large number of small localized shim coils has been proposed to address this issue and was shown to be more effective than SH shimming in the mouse (Juchem et al., 2011b) and human (Juchem et al., 2011a) brain. However, it requires an additional shim coil array outside (Juchem et al., 2011b) or inside (Juchem et al., 2011a) the radiofrequency (RF) coil, which takes up valuable space in the magnet bore and increases the distance between the subject and the shim coil array or the RF coil, respectively, resulting in a reduced shimming efficiency (i.e., magnetic field amplitude per unit current) or signal-to-noise ratio (SNR). In the latter case, a large (i.e., 10-cm) gap is also required in the shim coil array to allow RF penetration and to reduce RF damping (Juchem et al., 2011a), which further compromises the shimming performance. An alternative method based on a cylindrical network of actively controlled solid-state switches rather than a set of electrical coils has also been proposed (Harris et al., 2013), but still requires a separate shim coil array outside or inside the RF coil.

To address these limitations, we first proposed a new concept termed integrated parallel reception, excitation, and shimming (iPRES) (Han et al., 2012, 2013a, 2013b), which relies on a novel coil design that allows an RF current and a direct current (DC) to flow in the same coil simultaneously, thereby enabling parallel RF excitation/reception and localized B_0 shimming with a single coil array. Such an integrated RF/shim coil array can thus save valuable space in the magnet bore and be placed close to the subject to maximize both the SNR and shimming performance.

The feasibility of this approach was demonstrated in proof-of-concept experiments performed in a phantom with a single loop (Stockmann et al., 2013) or a two-coil array (Han et al., 2013a) and numerical simulations performed in the human brain with a 32-coil array (Stockmann et al., 2013) or a 48-coil array (Han et al., 2013a). In the present study, we further validate it by experimentally demonstrating its ability to perform parallel reception and localized B_0 shimming in the human brain in vivo. Preliminary results from our group (Truong et al., 2014) and from another group (Stockmann et al., 2014) have been presented in abstract form.

2. Methods

2.1 Integrated RF/Shim Coil Array Design

An integrated RF/shim coil array was built by modifying a 32-channel receive-only head coil array based on a gapped design (Ledden et al., 2007) and consisting of eight strips of four overlapping RF coils closely placed around the head (Fig. 1A). The coil array had an inner diameter of 20 cm in the right/left direction and 22 cm in the anterior/posterior direction. The approximate width and height of each coil ranged from 5 × 7 cm at the top of the head to 7 × 5 cm at the eyes level. Such a close-fitting coil array was chosen to maximize both the SNR and shimming efficiency, while still fitting all of our subjects and

leaving enough room around the head for foam padding or headphones (Fig. 1B). The healthy adult volunteer shown in Fig. 1B had a head circumference of 60 cm, which is above the 90th percentile for a height of 180 cm (Bushby et al., 1992). As such, our coil array is expected to fit the vast majority of subjects.

In our first implementation and without loss of generality, the 16 RF coils surrounding the anterior half of the brain (shown in color in Fig. 1A) were modified to enable parallel reception and localized B_0 shimming in the frontal brain region, which is affected by large susceptibility-induced B_0 inhomogeneities. For each coil, an inductor L_1 = 470 nH (Murata Manufacturing Co., Nagaokakyo, Japan) and a DC power supply were added to allow a DC current to flow in the closed loop (Fig. 1C), thereby generating a local magnetic field in the head coil array that can be used for B_0 shimming. The DC power supply, which was located outside the scanner room, was connected through two chokes L_2 = 470 nH and a shielded twisted-pair cable to prevent RF leaking and electromagnetic interference, respectively. A capacitor C = 180 pF was also added in shunt with the chokes to create a high-pass series pi network, keeping the RF resonant structure in tune. No additional RF chokes were used on the DC cables, which were braided and carefully routed to ensure that they did not cross any other element in the coil array and did not distort the RF field. The DC resistance of each RF/shim coil was 1.5 Ω. The coils were tuned and matched with a vector network analyzer (ZNB4, Rohde & Schwarz, Munich, Germany) and their unloaded and loaded quality factors Q_{UL} and Q_L were measured before and after converting the original RF coils to RF/shim coils.

Four dual-output DC power supplies (E3648A, Agilent Technologies, Cary, NC) operating in the constant-current mode with a maximum voltage rating of 8 V were used, thus providing eight independent DC currents. As a first approximation, the susceptibility-induced B_0 inhomogeneities in the brain were assumed to be symmetrical in the right–left direction, so that the same DC current was applied in coils symmetrically located on the right and left sides of the brain (shown with the same color in Fig. 1A).

The PIN diode on the left of Fig. 1C is used for active detuning during RF transmission and is biased from the scanner side through the DC voltage carried by the RF line. After converting the original RF coils to RF/shim coils, a 22 dB isolation can still be achieved when this PIN diode is biased, thus ensuring that the coils remain completely detuned during RF transmission.

2.2 Phantom Experiments

All experiments were performed on a 3 T MR750 MRI scanner (GE Healthcare, Milwaukee, WI). A one-time calibration was first performed on a 17-cm diameter spherical gel phantom. After second-order shimming with the SH shim coils of the scanner, a B_0 map was acquired without DC currents and eight B_0 maps were acquired with a DC current of 1 A separately applied in each pair of RF/shim coils. The first B_0 map was then subtracted from the other ones to remove any residual B_0 inhomogeneities due to imperfect shimming, resulting in eight basis B_0 maps, each representing the magnetic field per unit current generated by one pair of coils.

The B_0 maps were acquired with a multi-echo gradient-echo sequence (slice orientation = axial, repetition time (TR) = 530 ms, echo times (TEs) = 1.5, …, 11.2 ms, echo train length = 8, echo spacing = 1.4 ms, flip angle = 12°, field-of-view (FOV) = 25.6 × 25.6 cm, matrix size = 64 × 64, slice thickness = 4 mm, number of slices = 40, scan time = 34 s) and were computed with a voxel-wise linear regression of the phase images acquired at different TEs.

To demonstrate that the SNR was not compromised by the modifications made to the original RF coils, SNR maps were also computed from the magnitude images acquired at TE = 1.5 ms without DC currents as the signal intensity divided by the standard deviation of the noise in a background region. Separate SNR maps were computed by using the images reconstructed from each RF/shim coil surrounding the anterior half of the phantom and from each conventional RF coil surrounding the posterior half of the phantom. Furthermore, to demonstrate that the integrated RF/shim coil array can provide a comparable SNR as an unmodified commercial head coil array, SNR maps were also acquired with another close-fitting 32-channel receive-only head coil array (Nova Medical, Wilmington, MA) with an inner diameter of 19 cm in the right/left direction and 22 cm in the anterior/posterior direction. These SNR maps were acquired with the same phantom, pulse sequence, and slice positions, and were computed with the same method as described above by using the images reconstructed from each RF coil element. In addition, to demonstrate the temporal stability of the magnetic fields generated by the RF/shim coils, the calibration was repeated on two different days. Note that the coil array rigidly attaches to the patient bed at the same location for every scan, thus ensuring that there are no uncertainties in the B_0 maps due to the coil positioning.

2.3 Human Experiments

We carried out systematic investigations in healthy adult volunteers, who provided written informed consent to participate in this study under a protocol approved by our Institutional Review Board. After second-order shimming of the whole brain with the SH shim coils of the scanner, a B_0 map of the brain was acquired without DC currents by using the same method as described above, except that it was further smoothed with a 3×3×3 boxcar filter.

For each slice, the optimal DC currents to shim the anterior half of the brain were computed by minimizing the root-mean-square error (RMSE) in that brain region between the B_0 map acquired in vivo and a linear combination of the basis B_0 maps acquired in the phantom. The DC currents were constrained within a range of ±2 A in the optimization, as the inductors L_1 and L_2 were rated for a maximum DC current amplitude of 2 A. All computations were performed in Matlab (The MathWorks, Natick, MA) and the computation time for the DC current optimization was 34 s for all slices.

B_0 maps were then acquired with these optimal DC currents applied in the RF/shim coils. Since this first implementation did not include a dynamic shimming capability (i.e., the ability to update the optimal DC currents in real time for the acquisition of each slice (Blamire et al., 1996)), four separate B_0 maps were acquired with different sets of DC currents optimized to shim one out of four representative axial slices. The B_0 RMSE in the anterior half of the brain was then measured in all B_0 maps to quantify the shimming performance.

In addition, to demonstrate that the integrated RF/shim coil array can be used to actually correct for geometric distortions, one echo-planar imaging (EPI) dataset was acquired without DC currents and four EPI datasets were acquired with the same sets of optimal DC currents as those used for the B_0 maps. The images were acquired with a spin-echo single-shot EPI sequence (TR = 4.4 s, TE = 64 ms, FOV = 25.6 × 25.6 cm, matrix size = 128 × 128, slice thickness = 4 mm, frequency-encoding direction = right–left, partial-Fourier encoding = 5/8, sensitivity encoding (SENSE) acceleration factor = 2, number of averages = 1). For anatomical reference, undistorted T_2-weighted images were also acquired without DC currents with a fast spin-echo sequence (TR = 4.4 s, TE = 64 ms, echo train length = 8, FOV = 25.6 × 25.6 cm, matrix size = 256 × 192, slice thickness = 4 mm, SENSE acceleration factor = 2). Contour lines were then derived from these images and overlaid on the EPI images.

3. Results

Converting the original RF coils to RF/shim coils did not significantly impact their Q factor (Fig. 2A) or SNR (Figs. 2B,C). The unloaded-to-loaded Q ratios (Q_{UL}/Q_L) for a representative coil were 57.9/33.8 = 1.71 and 53.5/29.8 = 1.80 before and after the coil modification, respectively. In addition, the RF/shim coils (Fig. 2B) and conventional RF coils (Fig. 2C) of the integrated RF/shim coil array also had a comparable SNR as the RF coils of the commercial 32-channel head coil array (Fig. 2D). The slight difference in diameter between both coil arrays in the right/left direction should not significantly affect this SNR comparison. The 16 RF/shim coils were able to generate magnetic fields with different spatial patterns that can be combined and used for localized B_0 shimming (Fig. 3).

Even after second-order SH shimming of the whole brain, large susceptibility-induced B_0 inhomogeneities remained in the frontal brain region (Fig. 4A), resulting in severe geometric distortions in the EPI images (Fig. 5A, arrows). For each slice, the integrated RF/shim coil array was able to generate a localized magnetic field with a similar spatial distribution but an opposite polarity (Fig. 4B) to drastically reduce these B_0 inhomogeneities (Figs. 4C,D) and image distortions (Fig. 5B). For example, note how the anterior horns of the lateral ventricles are shifted back to their correct anatomical location With the 2D multislice acquisition and slice-specific shimming used in this work, the B_0 RMSE in the anterior half of the brain across 30 slices covering the whole brain was reduced by 60.3% (from 48.4 to 19.2 Hz). For comparison, with a 3D acquisition and whole-brain shimming, the B_0 RMSE in the same region would be reduced by 33.9% (from 48.4 to 32.0 Hz). Some residual B_0 inhomogeneities and image distortions remained (e.g., Fig. 5B, arrow) for the reasons discussed below.

The two sets of basis B_0 maps acquired on two different days were virtually identical (RMSE = 1.95 Hz) and the B_0 maps acquired in vivo with optimal DC currents (Fig. 4D) were in excellent agreement with those predicted from the shim optimization (Fig. 4C; RMSE = 4.95 Hz), thus demonstrating the temporal stability and reliability of the magnetic fields generated by the RF/shim coils. The average and maximum DC current amplitudes over all coils and all slices were 0.58 and 2.00 A, respectively. If the DC current amplitude were not limited to 2 A, these currents would be 0.63 and 2.99 A, respectively.

4. Discussion

The results of this study further validate previous proof-of-concept phantom experiments and numerical simulations (Han et al., 2013a; Stockmann et al., 2013) by experimentally demonstrating that the integrated RF/shim coil array can perform parallel reception and localized B_0 shimming in the human brain in vivo and that it can provide a much more effective shimming than SH shimming alone. Importantly, this method does not take up additional space in the magnet bore, does not compromise the SNR or shimming performance, and can be implemented with relatively simple modifications of a conventional RF coil array, unlike alternative methods requiring a separate shim coil array (Juchem et al., 2011a, 2011b; Biber et al., 2012; Harris et al., 2013).

In addition, using a close-fitting helmet coil array rather than a cylindrical coil array, as used in conventional multicoil shimming (Juchem et al., 2011a, 2011b), further increases both the SNR and shimming efficiency, because all of the RF/shim coils are closer to the head and because those located at the top of the head can generate a localized magnetic field within the brain (Fig. 3, bottom right) to shim deep B_0 inhomogeneities like those affecting the inferior frontal brain region. In contrast, a cylindrical coil array would require larger DC currents to achieve the same magnetic field at the center of the brain as well as opposite DC currents in adjacent coils to cancel out the magnetic field at the periphery. This higher shimming efficiency, along with the difference in field strength (3 T vs. 7 T) between our study and Juchem et al.'s study (2011a) explains why we were able to use a similar DC current range (±2 A vs. ±1 A) with only single-turn rather than 100-turn coils.

No significant heating, Lorentz forces, or eddy currents were observed in the RF/shim coils. Heating was evaluated with a temperature strip taped on the inner cover of the coil array across three adjacent RF/shim coils. When the maximum DC current of 2 A was applied in either one of these coils or all of the RF/shim coils, the temperature increased by 2°C or 4°C, respectively, within 10 minutes and remained stable afterwards. In the worst case scenario, the torque on a 5×7 cm RF/shim coil parallel to the B_0 field due to the Lorentz forces generated by the maximum DC current of 2 A at 3 T is only 0.021 Nm. Likewise, in the worst case scenario, the voltage induced by the maximum gradient amplitude of 50 mT/m and maximum slew rate of 200 T/m/s in a 5×7 cm RF/shim coil orthogonal to the B_0 field located 10 cm from the isocenter is only 70 mV. However, the actual voltage induced in the RF/shim coils measured during the EPI pulse sequence used in this work was only 13 ± 11 mV. More importantly, the DC power supplies operating in the constant-current mode were able to maintain the DC currents within 0.6 ± 0.4 mA from the prescribed values. As such, no additional modifications of the coils were required to minimize heating, Lorentz forces, or eddy currents.

The integrated RF/shim coil array built for this proof-of-concept study does have a few limitations. First, since only 16 RF/shim coils were used to shim the anterior half of the brain, minor B_0 inhomogeneities and image distortions remained in the posterior half of the brain, which was not included in the shim optimization. Second, since the same DC current was applied in coils symmetrically located on the right and left sides of the brain, residual B_0 inhomogeneities and image distortions remained in the anterior half of the brain, because

the susceptibility-induced B_0 inhomogeneities were not perfectly symmetrical in the right–left direction. Third, since the maximum DC current amplitude was limited to 2 A, residual B_0 inhomogeneities and image distortions also remained in the most inferior slice (Fig. 5B, arrow), for which some of the DC currents reached this limit in the constrained optimization. In addition, image distortions also remained in some of the skull/fat regions outside the brain, because these regions were closer to the RF/shim coils and were not included in the shim optimization (since they are not of interest for brain imaging). Fourth, since this first implementation did not include a dynamic shimming capability, separate B_0 maps and EPI datasets had to be acquired with different sets of DC currents optimized to shim different slices.

However, all of these limitations can be readily addressed without any technical obstacle in a full implementation (e.g., in an industrial solution for an actual product coil). The most straightforward extensions will be to use 32 RF/shim coils to shim the whole brain and to apply individually optimized DC currents in every coil to shim the right and left sides of the brain independently. In addition, the maximum DC current amplitude can be increased to improve the shimming performance in the most inferior slices. For example, increasing the maximum DC current amplitude to 3 A would allow an unconstrained shim optimization and further reduce the residual B_0 inhomogeneities and image distortions in the most inferior slice of Figs. 4 and 5. Alternatively, with the emergence of highly parallel 64-coil (Keil et al., 2013) or 96-coil (Wiggins et al., 2009) arrays, the number and density of RF/shim coils can also be increased to improve the shimming performance without necessarily increasing the maximum DC current amplitude. Finally, dynamic shimming can be implemented by adding an interface between the scanner and the programmable DC power supplies to update the optimal DC currents in real time for the acquisition of each slice, which has been demonstrated for conventional multicoil shimming (Juchem et al., 2011a, 2011b). The low inductance of each RF/shim coil (146 nH) and fast response time of the DC power supplies allow the DC currents to be switched from 0 to 2 A in about 50 μs, which is sufficiently fast for dynamic shimming.

While the integrated RF/shim coil array used in this study was built by modifying a conventional RF coil array, so that its design was constrained by the existing coil geometry, the shimming performance can be further improved by simultaneously optimizing the RF and DC performances of the coil array during the coil design (e.g., by optimizing the size and geometry of the coil array or the number, size, location, and geometry of the coil elements). Furthermore, while the integrated RF/shim coil array used in this study was designed for the human brain and used to reduce geometric distortions in EPI images, integrated RF/shim coil arrays can also be designed for other body parts for both human and animal applications and be used to correct for other types of artifacts, such as blurring in non-Cartesian imaging or signal loss in gradient-echo imaging. Finally, as demonstrated in previous phantom experiments (Han et al., 2013a), integrated RF/shim coil arrays can also be used for parallel excitation in addition to parallel reception and B_0 shimming, which may be useful for some ultra-high field applications.

In conclusion, the integrated RF/shim coil array can perform parallel reception and localized B_0 shimming in the human brain in vivo and provide a much more effective shimming than

conventional SH shimming without compromising the SNR or shimming performance. This method should be valuable for a wide range of applications requiring a high B_0 homogeneity.

Acknowledgments

We thank Saban Kurucay at GE Healthcare for helpful discussions. This work was in part supported by grants R01EB012586 and R01EB009483 from the National Institutes of Health.

References

Biber S, Wohlfarth K, Kirsch J, Schmidt A. Design of a local shim coil to improve B0 homogeneity in the cervical spine region. Proc. Intl. Soc. Mag. Reson. Med. 2012; 20:2746.

Blamire AM, Rothman DL, Nixon T. Dynamic shim updating: a new approach towards optimized whole brain shimming. Magn. Reson. Med. 1996; 36:159–165. [PubMed: 8795035]

Bushby KMD, Cole T, Matthews JNS, Goodship JA. Centiles for adult head circumference. Arch. Dis. Child. 1992; 67:1286–1287. [PubMed: 1444530]

Han H, Song AW, Truong T-K. Integrated parallel reception, excitation, and shimming (iPRES). Magn. Reson. Med. 2013a; 70:241–247. [PubMed: 23629974]

Han, H.; Truong, T-K.; Song, AW. Magnetic resonance imaging systems for parallel transmit, receive and shim and methods of use thereof. 2012. U.S. provisional patent application 61/665,517 filed June 28, 2012; U.S. patent application 13/898,993 filed May 21, 2013

Han, H.; Truong, T-K.; Song, AW. Magnetic resonance imaging systems for integrated parallel reception, excitation and shimming and related methods and devices. 2013b. International patent application PCT/US2013/042020 filed May 21, 2013

Harris CT, Handler WB, Chronik BA. A new approach to shimming: The dynamically controlled adaptive current network. Magn. Reson. Med. 2013; 71:859–869.

Hsu J-J, Glover GH. Mitigation of susceptibility-induced signal loss in neuroimaging using localized shim coils. Magn. Reson. Med. 2005; 53:243–248. [PubMed: 15678531]

Juchem C, Brown PB, Nixon TW, McIntyre S, Boer VO, Rothman DL, de Graaf RA. Dynamic multi-coil shimming of the human brain at 7 T. J. Magn. Reson. 2011a; 212:280–288. [PubMed: 21824794]

Juchem C, Brown PB, Nixon TW, McIntyre S, Rothman DL, de Graaf RA. Multicoil shimming of the mouse brain. Magn. Reson. Med. 2011b; 66:893–900. [PubMed: 21442653]

Keil B, Blau JN, Biber S, Hoecht P, Tountcheva V, Setsompop K, Triantafyllou C, Wald LL. A 64-channel 3T array coil for accelerated brain MRI. Magn. Reson. Med. 2013; 70:248–258. [PubMed: 22851312]

Ledden PJ, Mareyam A, Wang S, van Gelderen P, Duyn J. 32 channel receive-only SENSE array for brain imaging at 7T. Proc. Intl. Soc. Mag. Reson. Med. 2007; 15:242.

Romeo F, Hoult DI. Magnet field profiling: analysis and correcting coil design. Magn. Reson. Med. 1984; 1:44–65. [PubMed: 6571436]

Stockmann JP, Witzel T, Blau J, Polimeni JR, Zhao W, Keil B, Wald LL. Combined shim-RF array for highly efficient shimming of the brain at 7 Tesla. Proc. Intl. Soc. Mag. Reson. Med. 2013; 21:665.

Stockmann JP, Witzel T, Keil B, Mareyam A, Polimeni J, LaPierre WC, Wald LL. A 32ch combined RF-shim brain array for efficient B0 shimming and RF reception at 3T. Proc. Intl. Soc. Mag. Reson. Med. 2014; 22:400.

Truong T-K, Clymer BD, Chakeres DW, Schmalbrock P. Three-dimensional numerical simulations of susceptibility-induced magnetic field inhomogeneities in the human head. Magn. Reson. Imaging. 2002; 20:759–770. [PubMed: 12591571]

Truong T-K, Darnell D, Song AW. Integrated RF/shim coil array for parallel reception and localized B_0 shimming in the human brain at 3T. Proc. Intl. Soc. Mag. Reson. Med. 2014; 22:4849.

Wiggins GC, Polimeni JR, Potthast A, Schmitt M, Alagappan V, Wald LL. 96-Channel receive-only head coil for 3 Tesla: design optimization and evaluation. Magn. Reson. Med. 2009; 62:754–762. [PubMed: 19623621]

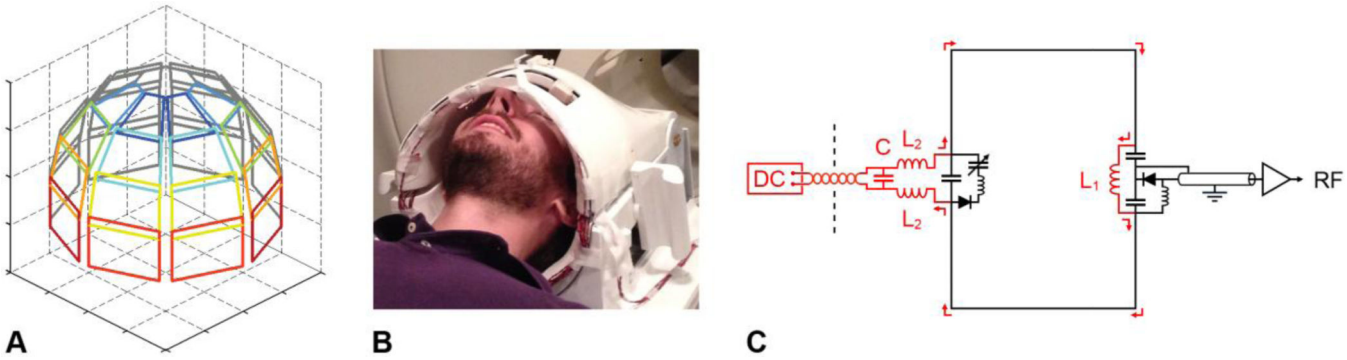

Fig. 1.

(A) Schematic diagram of the integrated RF/shim coil array, consisting of 16 conventional RF coils surrounding the posterior half of the brain (shown in gray) and 16 RF/shim coils surrounding the anterior half of the brain (shown in color), with the same DC current applied in coils symmetrically located on the right and left sides of the brain (shown with the same color). (B) Picture of the integrated RF/shim coil array. (C) Schematic diagram of one of the RF/shim coils, consisting of the original RF coil (shown in black) and the inductor L_1, chokes L_2, capacitor C, shielded twisted-pair cable, and DC power supply (shown in red) added to allow a DC current to flow in the closed loop (red arrows).

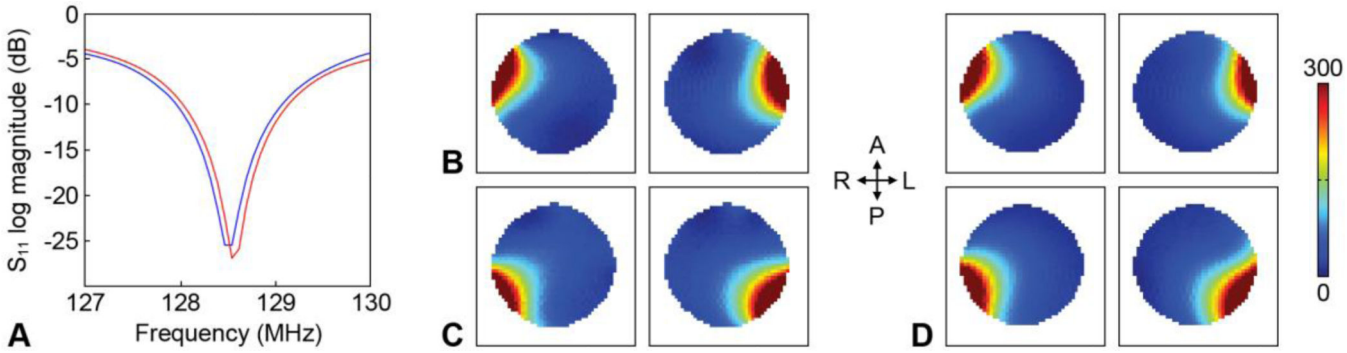

Fig. 2.

(A) S_{11} parameter of a representative loaded coil before (blue curve) and after (red curve) converting the original RF coil to an RF/shim coil. SNR maps in the same axial slice from two representative RF/shim coils (B) and two representative conventional RF coils (C) of the integrated RF/shim coil array and from four representative RF coils of the commercial 32-channel head coil array (D). The two coils in (B) are shown in orange in Fig. 1A, the two coils in (C) are those adjacent to them in the posterior direction, and the four coils in (D) were chosen to match the location of the four coils in (B) and (C). A: anterior, P: posterior, R: right, L: left.

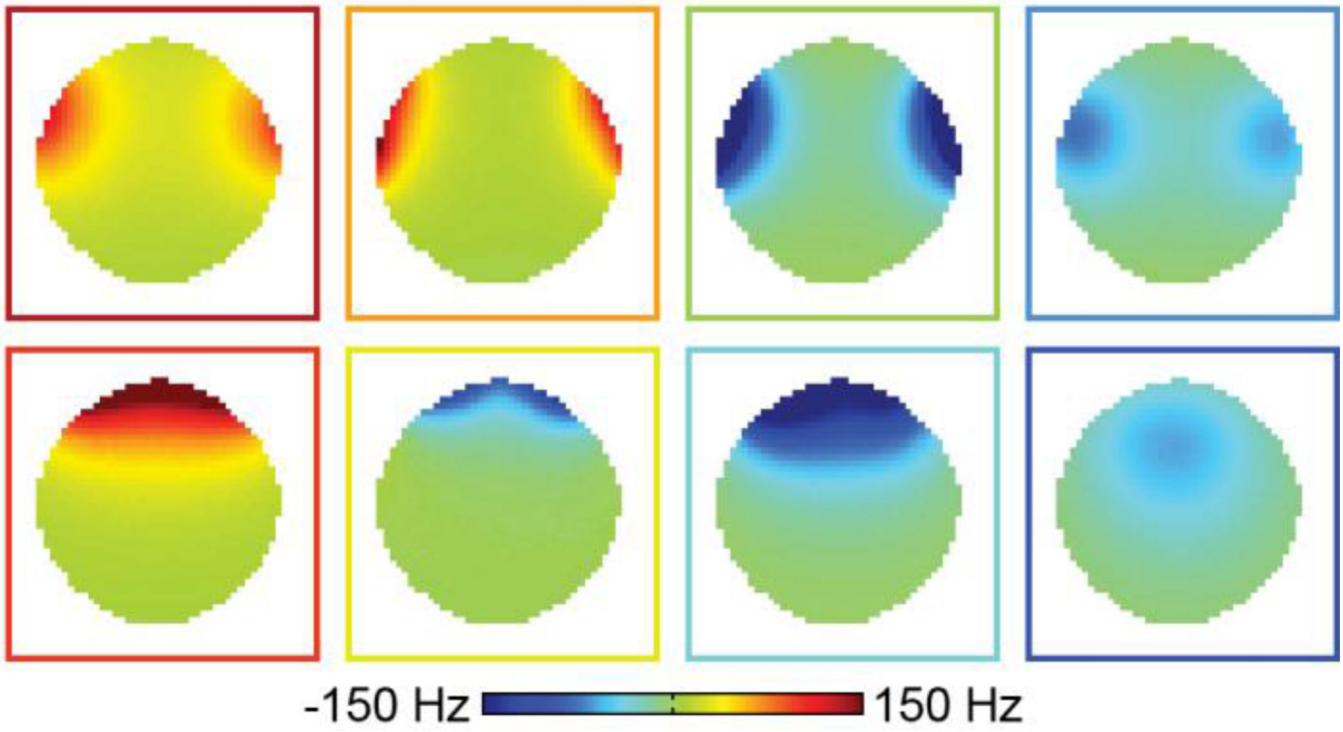

Fig. 3.

Basis B_0 maps acquired in a phantom with a DC current of 1 A separately applied in each pair of RF/shim coils. The color of the outline of each B_0 map matches the color of the RF/shim coils shown in Fig. 1A.

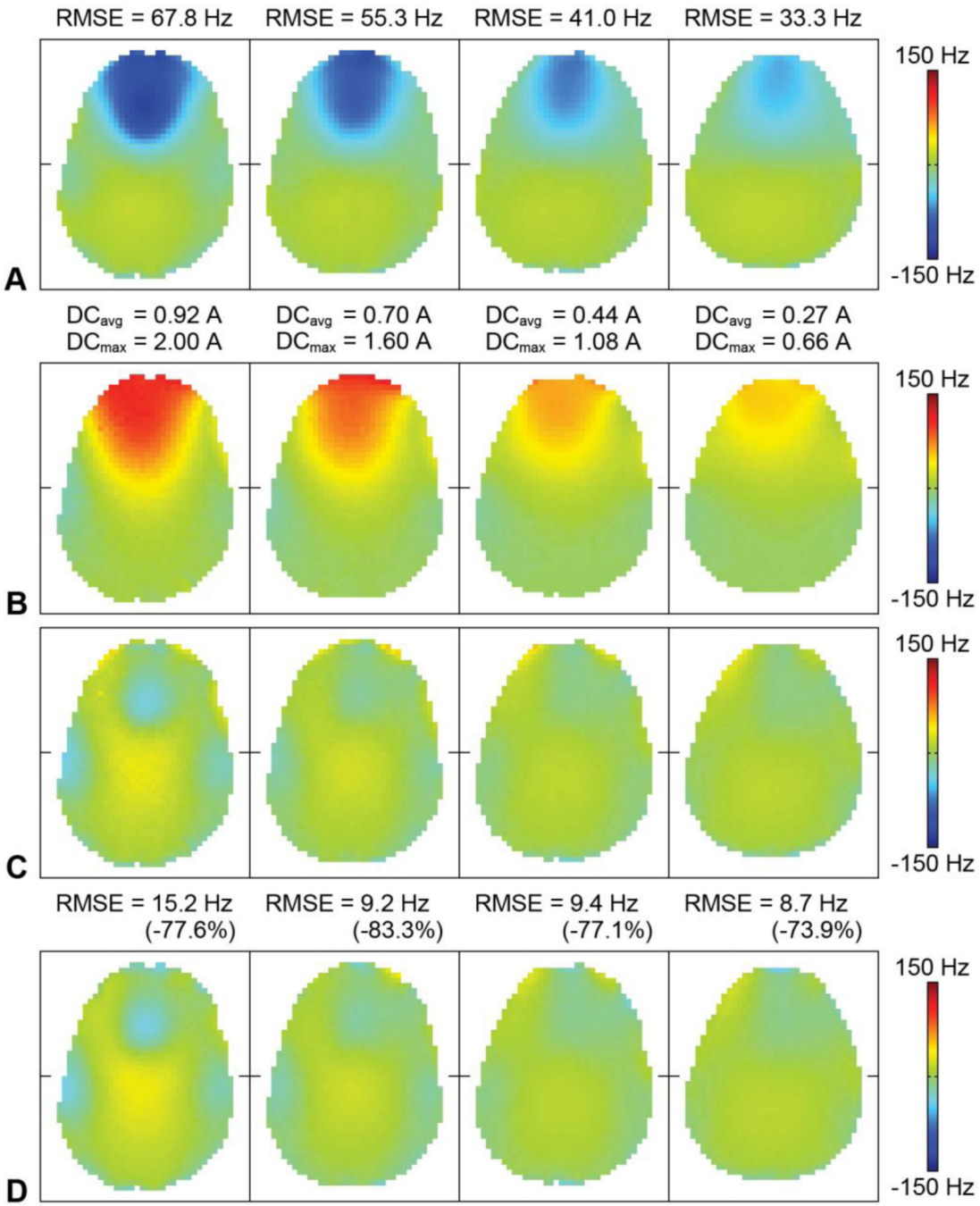

Fig. 4.

(A) B_0 maps acquired in vivo without DC currents in four representative slices. The B_0 RMSE in the anterior half of the brain is shown at the top. (B) B_0 field generated by the RF/shim coils with optimal DC currents (i.e., sum of the basis B_0 maps weighted by the optimal DC currents). The average and maximum DC current amplitudes applied in the RF/shim coils are shown at the top. (C) B_0 maps with optimal DC currents predicted from the shim optimization (i.e., sum of (A) and (B)). (D) B_0 maps acquired in vivo with optimal DC

currents. The B_0 RMSE in the anterior half of the brain and percent reduction with respect to (A) are shown at the top.

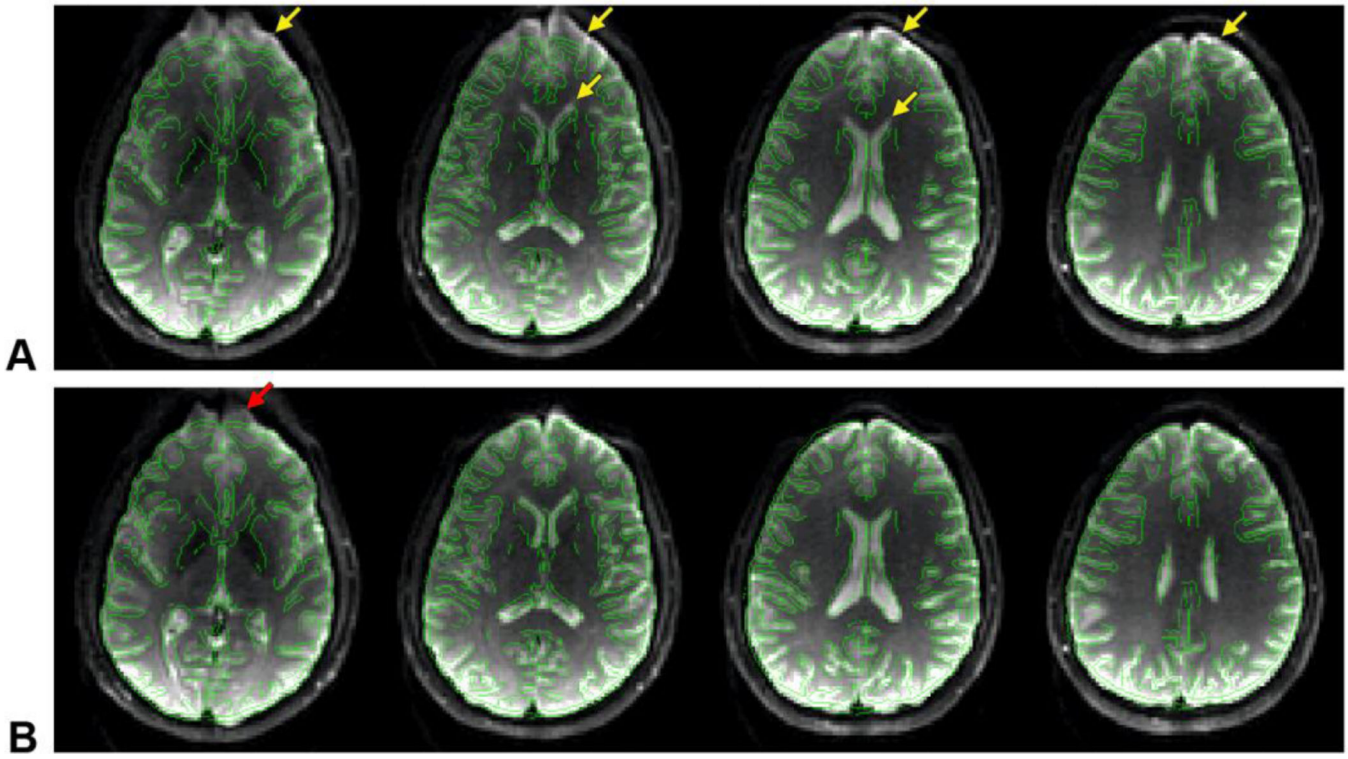

Fig. 5.

EPI images acquired in the same slices as in Fig. 4 without DC currents (A) and with optimal DC currents (B), with overlaid contour lines derived from the undistorted fast spin-echo images. The arrows point to susceptibility-induced distortions in the frontal brain region.